Earth and Planetary Science Letters 604 (2023) 117977

Contents lists available at ScienceDirect

Earth and Planetary Science Letters

journal homepage: www.elsevier.com/locate/epsl

Predicting turbidity current activity offshore from meltwater-fed river deltas

Lewis P. Bailey [a,b,c,*], Michael A. Clare [a], Ed L. Pope [d], Ivan D. Haigh [b], Matthieu J.B. Cartigny [d], Peter J. Talling [d], D. Gwyn Lintern [e], Sophie Hage [f], Maarten Heijnen [a]

[a] National Oceanography Centre, Southampton, UK
[b] School of Ocean and Earth Science, University of Southampton, UK
[c] Department of Geoscience, University of Calgary, AB, Canada
[d] Departments of Geography and Earth Science, Durham University, UK
[e] Natural Resources Canada, Geological Survey of Canada, Sidney, BC, Canada
[f] Univ Brest, CNRS, Ifremer, Geo-Ocean, Plouzané, France

ARTICLE INFO

Article history:
Received 9 August 2022
Received in revised form 30 November 2022
Accepted 23 December 2022
Available online xxxx
Editor: J.-P. Avouac

Keywords:
submarine channel
turbidity current
multivariate analysis
triggering
prediction

ABSTRACT

Quantification of the controls on turbidity current recurrence is required to better constrain land to sea fluxes of sediment, carbon and pollutants, and design resilient infrastructure that is vulnerable to such flows. This is particularly important offshore from river deltas, where sediment supply is high. Numerous mechanisms can trigger turbidity currents, even at a single river mouth. However quantitative analysis of recurrence and triggers has been limited to an individual trigger for each turbidity current due to the low number of precisely timed (via direct monitoring) flows. We are therefore yet to quantify if and how coincident processes combine to generate turbidity currents, and their relative importance. Here, we analyse the timing and causes of 113 turbidity currents directly-monitored from the source of turbidity current initiation to depositional sink in a single submarine channel. This submarine channel is located offshore from glacial-fed river-deltas at Bute Inlet, a fjord in British Columbia, Canada. Using a multivariate statistical approach, we demonstrate the statistical significance of combined river discharge and tidal controls on turbidity current occurrence during 2018, from which we derive a statistical model that calculates turbidity current probability for any given input of river discharge and water level. This new model predicts turbidity current activity with >84% success offshore other river deltas where flow timing is precisely constrained by directly monitoring, including the Squamish and Fraser River-deltas in British Columbia. We suggest that this model will be applicable for turbidity current prediction at glacial meltwater-fed fjords in many other regions worldwide.

© 2023 The Author(s). Published by Elsevier B.V. This is an open access article under the CC BY license (http://creativecommons.org/licenses/by/4.0/).

1. Introduction

Submarine sediment flows, known as turbidity currents, sculpt the deepest canyons (Harris and Whiteway, 2011; Shepard, 1972) and form some of the largest sediment accumulations on our planet (Talling, 2014). Turbidity currents dominate the transport and burial of terrestrial derived sediments (Talling, 2014), organic matter (Dai et al., 2012; Galy et al., 2007; Hage et al., 2022, 2020; Lee et al., 2019), and pollutants, such as litter (Pierdomenico et al., 2019; Zhong and Peng, 2021) and plastics (Pierdomenico et al., 2022; Pohl et al., 2020), to deep ocean basins. Due to their often-high velocities and long runout distances, turbidity currents pose a significant hazard to important seafloor infrastructure such as telecommunications cables (Carter et al., 2012; Heezen and Ewing, 1952; Piper et al., 1999; Talling et al., 2022). However, there are very few turbidity current systems where flow timings are precisely known (e.g. Bailey et al., 2021; Clare et al., 2016), and even fewer locations where there is also information on the final runout distance of these flows (Hizzett et al., 2018; Pope et al., 2022; Talling et al., 2022). Most previous work has focused on how a single external factor may trigger turbidity currents, such as earthquakes (Howarth et al., 2021) or river floods (Mulder et al., 2003). However, numerous mechanisms are capable of triggering turbidity currents, even within a single system (Bailey et al., 2021; Canals et al., 2006; Carter et al., 2012; Clare et al., 2016; Gavey et al., 2017;

* Corresponding author at: Department of Geoscience, University of Calgary, AB, Canada.
E-mail address: Lewis.Bailey@ucalgary.ca (L.P. Bailey).

https://doi.org/10.1016/j.epsl.2022.117977
0012-821X/© 2023 The Author(s). Published by Elsevier B.V. This is an open access article under the CC BY license (http://creativecommons.org/licenses/by/4.0/).

Khripounoff et al., 2009). Despite this, the number of turbidity currents recorded at a single site via direct monitoring has limited statistical analysis to univariate approaches (i.e. the role of a single triggering mechanism in isolation on turbidity current generation). As such, we are yet to quantify robustly: (1) how multiple possible coincident triggers can combine to generate turbidity currents; (2) the relative importance of different triggers where multiple mechanisms may be responsible for generating turbidity currents in a single system, and; (3) whether turbidity current runout is controlled by the type of trigger, its magnitude, or a combination of multiple triggers. Statistical analysis of a large number of turbidity currents measured at high-temporal resolution, and from point of turbidity current generation to depositional sink, is critical to address these outstanding issues. In turn, such analysis will advance our ability to predict turbidity current frequency, magnitude and timing to assess the threats posed to seafloor infrastructure, and to quantify the fluxes of sediment and associated particulate matter to the deep sea.

The mechanisms for turbidity current initiation have been best constrained offshore from river deltas. These mechanisms include: (1) Delta slope failures that generate submarine landslides which evolve downslope into turbidity currents (Clare et al., 2016; Hizzett et al., 2018; Prior et al., 1981); (2) Plunging of sediment-laden river flood water (hyperpycnal flows) that directly forms a turbidity current if the suspended sediment concentration exceeds the density of seawater (>40 $kg\,m^{-3}$; Carter et al., 2012; Khripounoff et al., 2009; Liu et al., 2012; Mulder and Syvitski, 1995); (3) Indirectly, from sediment settling-driven convection from a dilute plume (sediment concentrations as low as 1 $kg\,m^{-3}$; Parsons et al., 2001); (4) Turbidity currents initiate from exceptionally dilute river plumes (<1 $kg\,m^{-3}$) from sediment suspensions accumulating in the turbidity maximum zone are pushed offshore at low tide (Hage et al., 2019). A turbidity maximum occurs in tidal deltas where there can be increased levels of sediment concentration at the interface between the fresh river and more saline water offshore (Dyer, 1997).

Recent field-scale flow monitoring offshore from river mouths has recognised the combined effect of elevated river discharge and tidal drawdown on flow generation (Ayranci et al., 2012; Clare et al., 2016; Hage et al., 2019; Hill and Lintern, 2021; Hughes Clarke et al., 2012; Lintern et al., 2016; Talling et al., 2022). For example, elevated river discharge may rapidly deposit sediment on the delta-lip, thus preconditioning the delta slope to failure. The likelihood of failure is subsequently heightened at low tide when hydrostatic pore pressures decrease, due to the expansion of gas bubbles (e.g. Christian et al., 1997). High river discharge can also increase suspended sediment in the turbidity maximum; while forcing this turbidity maximum zone further away from the delta-lip by the promotion of faster flow at lower tides. Similarly, amplification of river flow velocity at low tide, especially during spring tide cycles, will also increase river bed shear stress resulting in enhanced erosion and flushing sediment from the delta top (Clare et al., 2016; Eidam et al., 2019). The mechanisms involved may vary, but the common theme is that the triggering of turbidity currents offshore from river deltas appears to be strongly controlled by a combination of both river discharge and tidal fluctuations. However, univariate statistical analysis has not allowed the investigation of multiple coincident environmental factors that combine (often in a non-linear manner or with threshold behaviours) to trigger flows. Moreover, 87% of the fluvial-marine sediment flux offshore from river deltas worldwide occurs at river and tide-dominated systems (Nienhuis et al., 2020). Therefore, understanding the controls of both river discharge and tidal fluctuations on turbidity current generation can provide an insight for the transfer of sediment, and its timing, between the land and ocean.

Through analysis of 113 turbidity currents where timing and runout distance is well constrained via direct monitoring, we use a multivariate statistical approach to investigate the relative importance of river discharge and tides, and how these combine, to trigger turbidity currents. Instrument moorings were deployed in the submarine channel at Bute Inlet, a glacial meltwater-fed fjord, located in British Columbia, Canada (Fig. 1). Precise (up to four second-resolution) turbidity current timing was recorded using six Acoustic Doppler Current Profilers (ADCPs) from the Homathko River Delta to the channel-lobe over two separate deployment campaigns during 2016 and 2018 (Table S1). The speeds and internal structure of these flows were recently analysed by Pope et al. (2022), but that study did not include assessment of flow timing, frequency or triggers. The precisely-recorded flow timings, along with monitoring of the river discharge and tidal elevation at the time of flow initiation, are used to investigate turbidity current triggering and runout. From this analysis, we develop and validate a novel multivariate statistical framework for predicting turbidity current timing at Bute Inlet using the dataset from 2018. We then demonstrate its predictive power, by hindcasting turbidity current activity (i.e. timing of turbidity currents and periods without turbidity currents) in Bute Inlet during 2016 and on similar, but unrelated, systems (Fraser River and Squamish Deltas; Fig. 1 inset). We finally discuss how our statistical approach may provide a basis to predict the timing of turbidity current activity beyond Bute Inlet, and where else the predictive model may be applicable.

2. Geographic setting

Bute Inlet lies within the Pacific Ranges of the Coast Mountains of British Columbia, Canada. The coastal environment of the region is macrotidal, predominantly semidiurnal, with a range of 5 m. Mountains exceeding elevations of 3000 m are common, with many maintaining small ice caps and valley glaciers (Holland, 1976) within the drainage basins of the Homathko and Southgate Rivers. The Homathko River has an average discharge of 250 $m^3\,s^{-1}$, but often exceeds daily discharge maxima of 1,000 $m^3\,s^{-1}$, during the May to August freshet season due to glacial melt, decreasing to ~50 $m^3\,s^{-1}$ in January to February. Peaks in discharge typically also occur in late October to November following periods of intense rainfall. Estimates of maximum suspended sediment concentrations for the Homathko River are 0.5-0.7 $kg\,m^{-3}$; such concentrations are not sufficient for wholescale plunging of (hyperpycnal) river floodwater (Bornhold et al., 1994; Mulder and Syvitski, 1995). The Southgate River has only been gauged since June 2021, with measurements of discharge approximately 50% of the Homathko River (Hage et al., 2022).

The delta fronts of the Homathko and Southgate Rivers are characterised by a series of subaqueous channels, which converge into two well-developed channels entering the fjord from opposite sides (Fig. 1). These two channels join, forming a single submarine channel that continues down-fjord for 40 km to a water depth of 660 m where the channel transitions to a depositional lobe (Conway et al., 2012; Heijnen et al., 2020). This submarine channel is highly active with tens of turbidity currents frequently occurring in the upper channel during the freshet (Bornhold et al., 1994; Heijnen et al., 2022; Pope et al., 2022), and therefore acts as an efficient mechanism for the transport and burial of organic carbon supplied by the Homathko and Southgate Rivers (Hage et al., 2022).

3. Data and methods

3.1. Instrument deployment

Turbidity current monitoring data were acquired from two separate field campaigns in Bute Inlet during 2016 (11th June to 10th

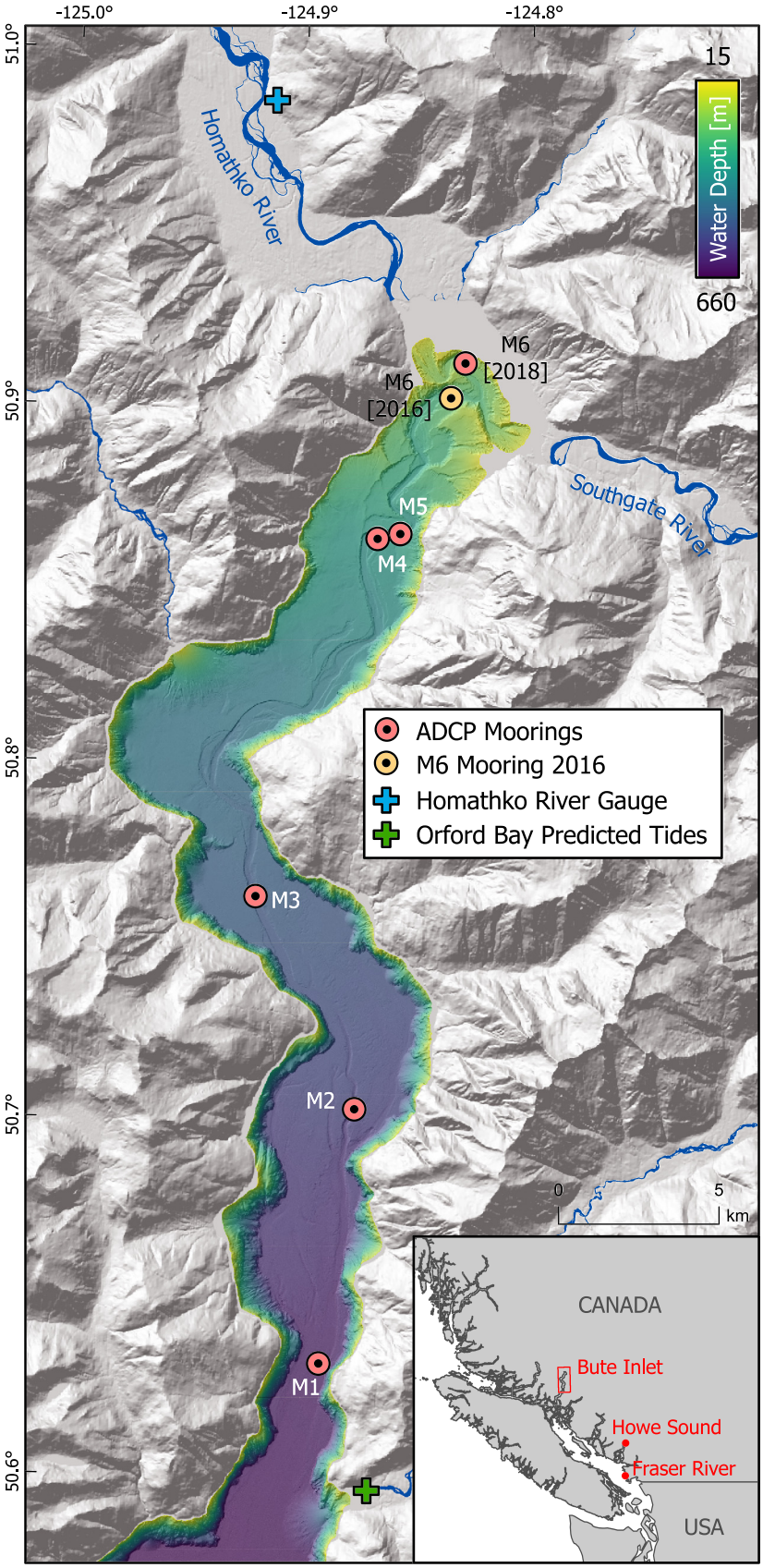

Fig. 1. Bathymetric map of the submarine channel in Bute Inlet, British Columbia, Canada. The locations moored ADCPs are shown (labelled M6 to M1) for both 2016 and 2018 deployments. The position of the Homathko River discharge gauge and site of tide predictions are also displayed.

October) and 2018 (15th May to 25th September). Six moorings (labelled M6 to M1 in Fig. 1) with downward looking ADCPs (with frequencies of 300 or 600 kHz, see Table S1) were deployed along the length of the submarine channel in each monitoring campaign, the positions of which were consistent apart from the uppermost mooring (M6) which was located ~2.5 km closer to the Homathko River Delta in 2018 (Fig. 1; Pope et al., 2022). The four shallowest ADCPs (M6 to M3) were suspended between two anchors placed on either side of the channel (see two-point moorings in Clare et al., 2020, for full details). The footprint of each ADCP sufficiently covered the width of the submarine channel. Measurements of water column velocity and backscatter were made at 4 or 6-second resolution in 0.5-1 m vertical intervals (Table S1). In 2016, velocity data was only recorded at M4, while M6 only made measurements for the first 50 days (~40%) of deployment. Water damage during deployment of M5 also meant no measurements could be made with this instrument made during the 2018 deployment.

3.2. Measuring turbidity currents and potential triggers

A turbidity current event is identified from the ADCP data by an abrupt increase in acoustic backscatter (i.e. increased suspended sediment) and an increase in down-channel velocity (Pope et al., 2022). Identification of a flow at sequential moorings down-channel provides a minimum runout distance. The detection time at M6 (the shallowest mooring) is taken as the timing of turbidity current initiation to compare to potential triggering mechanisms. We compare the timing of turbidity currents to: (1) Hourly discharge data of the Homathko River obtained from Environmental and Natural Resource Canada Station 08GD004 (https://wateroffice.ec.gc.ca), located 10 km upstream from the Homathko Delta. The Southgate River was not gauged during the period of the study so therefore could not be analysed; and (2) Water level estimates using tidal predictions for peak high and low tides at Orford Bay (http://tides.gc.ca; Fig. 1). A time series was produced by fitting a cubic interpretation to splice data into hourly measurements.

3.3. Univariate statistical analysis

Non-parametric Mann-Whitney-Wilcoxon and Kolmogorov-Smirnov tests are used to determine whether the distribution of Homathko River discharge and tidal elevation are significantly different at the time of turbidity currents to intervals that do not feature turbidity currents. Both tests have the advantage of not requiring the distribution of data a priori. The Kolmogorov-Smirnov test is sensitive to any differences (i.e. shape, spread or median) in the two distributions, whereas the Mann-Whitney-Wilcoxon test is sensitive to changes in the median. Statistically significant differences are defined when $p < 0.05$ (i.e. 95% significance level).

3.4. Logistic regression probability model

Logistic regression is suited to testing the relationship of a dichotomous outcome (i.e. the triggering of a turbidity current, or not) with one or more predictor variables by applying the logit transformation to the dependent variable (in this study the likelihood of a turbidity current; see Supplementary Material; Peng et al., 2002). We use logistic regression to estimate the relative contribution of Homathko River discharge and tidal elevations on the generation of turbidity currents (Fig. 2). Understanding this relationship in turn allows an estimation of turbidity current likelihood under given conditions of Homathko River discharge and water level.

Turbidity current activity in Bute Inlet does not always align with individual peaks in Homathko River discharge (Bornhold et al., 1994). Instead, turbidity current activity 'switches on' above a minimum discharge threshold (Clare et al., 2016). Therefore, the Homathko River discharge component of the logistic regression uses river discharge recorded during 2018 normalised to a percentile of 20 yrs of Homathko River discharge measurements (1999-2018). This normalised river discharge shows a greater data spread than the raw observations when Homathko River discharge is close to the 'switch on' threshold for turbidity current activity, while also decreasing the magnitude of large river discharge peaks. Reducing these peaks ensures our model does not overestimate turbidity current likelihood. This normalisation further allows the model to be applied to other turbidity current systems. Turbidity current activity is most favourable at low (spring) tide (Clare et al., 2016; Hage et al., 2019); however, water level in isolation is a poor predictor of turbidity current activity (see Section 4.1). For example, the same measurement of water level for different days may represent different positions in the tidal cycle. We therefore classify water level in a series of tidal modes for low (L), high (H), high-low (hL) and low-high (lH) positions in the semidiurnal tidal cycle. Each of these modes is defined as a 4 h period centred on slack water (Fig. 2). To ensure these windows do not overlap, L and H modes take priority, with hL and lH modes shortened. Where hL and lH modes overlap preference is taken to the closest tidal peak, and removed from the other window. Dummy coding each water level measurement then produces a categorical model input (i.e. if hourly measurement is within the low tide window $L = 1$, and all other modes H, hL, $lH = 0$). This is then multiplied by the corresponding tidal range (i.e. the distance between the closest neighbouring low and high-water levels) such that a higher value is observed during spring tides. We use these variables to apply a five-predictor logistic model, such that:

$$\hat{p}(\mathrm{TC}) = \frac{e^{\alpha+\beta_1 Q+\beta_2 L+\beta_3 H+\beta_4 hL+\beta_5 lH}}{1+e^{\alpha+\beta_1 Q+\beta_2 L+\beta_3 H+\beta_4 hL+\beta_5 lH}}, \quad (1)$$

where, $\hat{p}(\mathrm{TC})$ is the estimate of turbidity current occurrence probability, α (or y-intercept) and the βs are regression coefficients, Q is the percentile normalised Homathko River discharge, and L, H, hL and lH each refer to the tidal modes. Equation (1) is effectively a two-predictor logistic model, as only one of the tidal modes will have a non-zero value for a given measurement of water level.

Estimations of the α and β constants are calculated using the timing of turbidity currents recorded at M6 (Fig. 1, 2) during 2018 using the maximum likelihood method (see Supplementary Material). Here, each corresponding hourly measurement of percentile-normalised Homathko River discharge and categorical tidal modes throughout 2018 were assigned a value of $p(\mathrm{TC}) = 1$, where a turbidity current occurred within that hour, or $p(\mathrm{TC}) = 0$, when a turbidity current did not occur. As turbidity current activity is reduced, or switched off entirely, outside of the freshet (Bornhold et al., 1994), and the instrument deployment period aligned with the elevation of Homathko River discharge (Fig. 3B), the model assumes that no turbidity currents occurred outside the monitoring window. Once calculated, the probability of a turbidity current occurring can be estimated for any measurement of percentile of the normalised Homathko River discharge and categorical tidal mode (Fig. 2).

We evaluate the logistic model by using a series of statistical tests on the individual predictors and the overall model (Fig. 2). The statistical significance of individual regression coefficients (i.e. α and β constants) are tested using the Wald chi-squared (χ^2) statistic. The statistical significance of the coefficients is determined when $p < 0.05$ and $\chi^2 > 11.1$ (the critical χ^2 value for a logistic model with five – the number of predictor variables – degrees of freedom at the 95% significance level). To assess

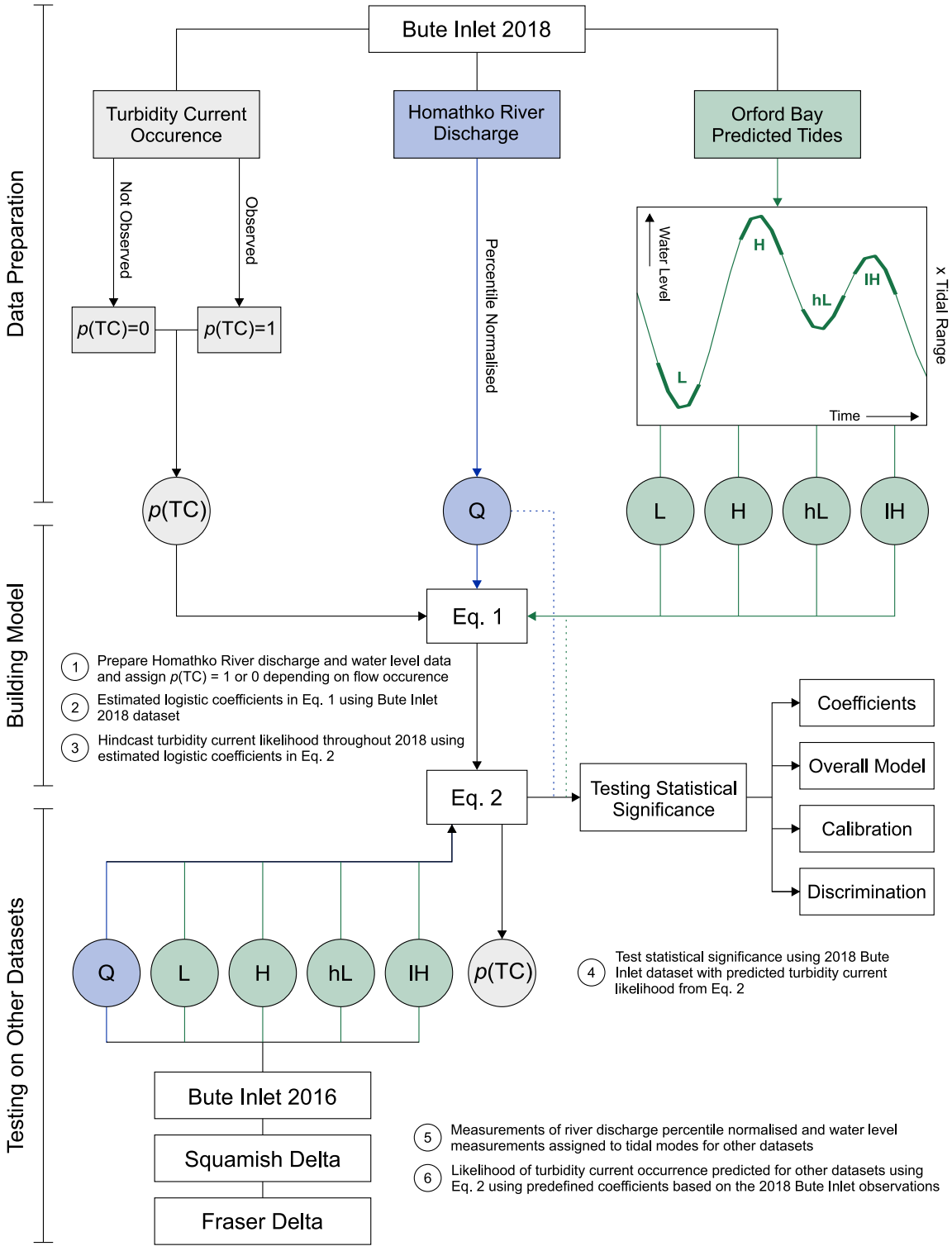

Fig. 2. Diagram to show the workflow to prepare river discharge and water level data, build and test the statistical significance of the logistic model, and then test on other independent datasets. Labels 1-6 describe the workflow procedure. Q refers to percentile normalised Homathko River Discharge; L the low tide mode; H, high tide; hL high-low tide; lH, low-high tide; and p(TC) the predicted probability of a turbidity current.

whether the overall model is an improvement over the null (i.e. where each parameter is equal to zero) we use the likelihood ratio and Wald tests. The null hypothesis is rejected and parameters are statistically significant if $p < 0.05$ and $\chi^2 > 3.84$ (critical χ^2 value for a single degree of freedom at the 95% significance level). The efficacy of the model calibration is assessed through comparison of estimated probabilities of turbidity current occurrence with the actual timing of flows during the 2018 monitoring campaign in Bute Inlet. We measure the fit of the logistic model using the Hosmer-Lemeshow test supplemented by the McFadden pseudo-R^2 (Lemeshow and Hosmer, 1982; McFadden, 1974). For more details on the tests used to evaluate the logistic model see Supplementary Material.

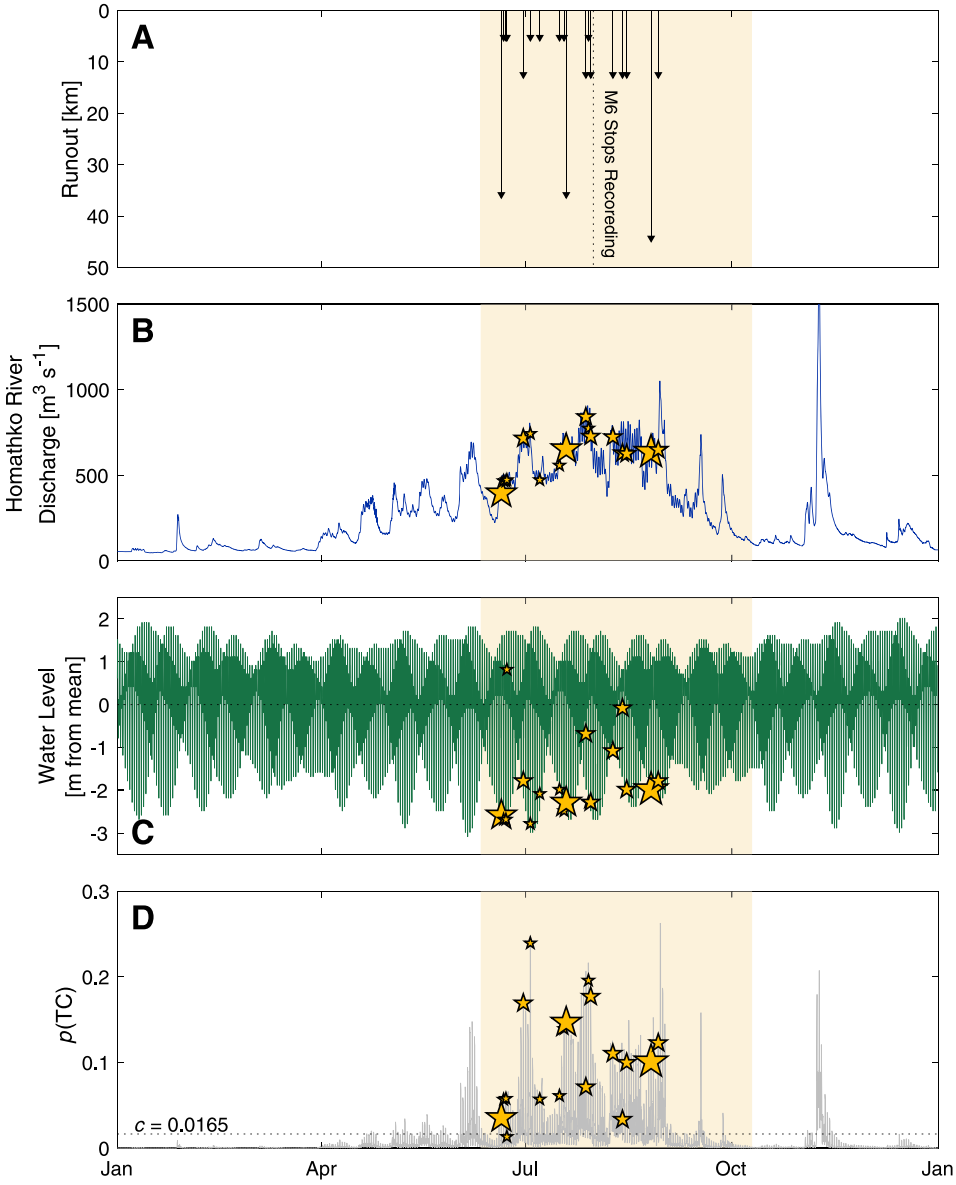

Fig. 3. Time series of recorded and calculated measurements during 2016 at Bute Inlet. (A) The timing of detected turbidity currents with minimum channel runout. (B) Homathko River discharge. (C) Deviation of water level from mean at Orford Bay. (D) Estimates for predicted probability of turbidity current occurrence from Eq. (2) (built using the 2018 Bute Inlet dataset) using Homathko River discharge and water level recorded during 2016. Yellow stars in B-D show the value of each variable during measured turbidity currents, the size of star is relative to minimum flow runout. Highlighted area denotes the period of instrument deployment, outside of which flow timing is unknown. Note most proximal mooring (M6) stopped recording 50 days into monitoring.

Model discrimination (i.e. ability to discriminate between events and non-events) assesses the predictive power of the logistic model (Fig. 2). For example, observations of turbidity currents ($Y = 1$) should be associated with high predicted probabilities and periods of no turbidity currents ($Y = 0$) with low predicted probabilities. The use of the logit function in logistic regression does not explicitly classify observations as positive (i.e. the occurrence of a turbidity current) or negative (i.e. non-events). We therefore select a cut point (c), and classify calculated probabilities above c as 'positive' (the occurrence of a turbidity current) and below as 'negative' (the absence of a turbidity current). The value of c is determined by model sensitivity and specificity, where sensitivity is the probability of predicting an observation as 'positive' given that $Y = 1$, and specificity is the probability of the model predicting a 'negative' given the actual outcome was $Y = 0$. We therefore choose a value of c where model sensitivity and specificity are equal. We use this c value to assess the overall predictive power of the logistic model i.e. the ability to correctly predict the monitored timing of actual turbidity currents, or absence of flows as 'positive' or negative' events. Model discrimination is further quantified using the concordance (or c-) statistic (see Supplementary Material).

3.5. Comparison of univariate and multivariate turbidity current prediction

Turbidity current timing was predicted using the logistic model (Eq. (2)), as well as using the Homathko River discharge and water level in isolation. We then compare predicted results with the actual timing of turbidity currents. To do this, a series 95 values (i.e. the number of turbidity currents measured during 2018) were each randomly selected from the top 10^{th} percentile of results from the logistic model, Homathko River discharge, and lowest 10^{th} percentile of water level observations. The Mann-Whitney-Wilcoxon and Kolmogorov-Smirnov tests are used to compare the distribution of Homathko River discharge and water level (both

annual range and during events) with each series of predicted outcomes. Here, a good prediction will show a statistically significant difference ($p < 0.05$) between predictions to the annual range of measurements (as shown in Section 4.1), and no statistically significant difference ($p > 0.05$) when comparing predictions to the measurements of Homathko River discharge and water level recorded during actual monitored turbidity currents. Offsets in distribution are further quantified as the difference between medians (DBM) as a percentage of overall visual spread (OVS), where OVS is the range from the lowest to highest interquartile (25^{th} and 75^{th} percentile) range (Bailey et al., 2021).

3.6. Testing the logistic model on other datasets

To validate our model, we first apply the logistic equation with coefficient values determined using the 2018 dataset in Bute Inlet to Homathko River discharge, tidal elevation and turbidity current timing recorded during a different period in 2016 (Fig. 2). We then assess the application of the predictive model (Fig. 2) to other sites using direct monitoring datasets from Squamish Delta, Howe Sound, in 2011 and Fraser River-Delta in 2008. Both of these river deltas are located in British Columbia, Canada (Fig. 1 insert). Previous work has demonstrated that turbidity current activity at both these locations is similarly focused during the spring and summer freshet, with preferential triggering at low tide (Ayranci et al., 2012; Clare et al., 2016; Hage et al., 2019; Hill and Lintern, 2021; Hughes Clarke et al., 2012; Lintern et al., 2016).

Both the Squamish and Fraser River-Deltas have physiographic similarities to Bute Inlet. Howe Sound is located ~180 km southeast of Bute Inlet with the Squamish and Homathko Rivers having comparable discharge, and grain sizes present on the delta fronts (Hickin, 1989). Three channels incise the Squamish Delta front, which extend seaward for ~2 km where each then terminates in a broader depositional lobe. A 600 kHz ADCP measuring at a 30 second temporal resolution, moored at the termination of the northern-most channel recorded precise timings of 22 turbidity currents during a 147-day deployment from March to August of 2011 (Clare et al., 2016; Hughes Clarke et al., 2012). The Fraser River is the largest river in western Canada, with a river discharge is an order of magnitude greater than the Homathko and Squamish Rivers. An instrumented platform, located 250 m seaward of the Fraser Delta, was deployed adjacent to the main submarine channel from January to October 2008. Three turbidity currents were directly monitored using a 150 kHz ADCP along with temperature, pressure, salinity and turbidity sensors during this period (Ayranci et al., 2012). For each site we compare modelled predicted probabilities with the timing of ADCP recorded turbidity currents using percentile-normalised measurements of river discharge and water level. Full details of data collection and preparation can be found in Supplementary Material. Using the c value calculated from the 2018 Bute Inlet dataset we quantify the predictive power of the logistic model as the probability of correctly predicting the 'positive' or 'negative' occurrence of turbidity currents.

4. Results

4.1. Turbidity current activity in Bute Inlet

A total of 113 turbidity currents were directly monitored in Bute Inlet using ADCPs during the freshet of 2016 (N = 18) and 2018 (N = 95) as recently documented by Pope et al. (2022). Most turbidity currents ran out for distances of 3.1-to-12.2 km along the channel, with only 22% of turbidity currents recorded beyond this, and only two (one per campaign) detected at the final mooring located 44.1 km down-channel on the terminal lobe (Figs. 1; 3A; 4A). During instrument deployment, all flows occurred when Homathko River discharge was above 230 $m^3 s^{-1}$. Large peaks in the flood hydrograph (>1500 $m^3 s^{-1}$ in 2016) were observed between October and November, relating to seasonal periods of intense rainfall (Figs. 3B; 4B). However, ADCPs were not deployed during this interval, and thus turbidity current activity relating to this seasonal rainfall remains unknown. While there is a link between river discharge and turbidity current activity, individual peaks in the Homathko River discharge during the freshet did not always result in turbidity currents (Figs. 3B; 4B). Turbidity current timing also shows a strong correlation with tides; 68% of flows occur at peak low tide and 60% when tidal range is increased relating to neap-to-spring tidal cycles (Figs. 3C; 4C). Univariate analysis further quantifies the role of Homathko River discharge and water level on turbidity current timing. Both variables show a significant statistical difference between conditions during turbidity currents and periods where turbidity currents were absent ($p < 0.05$ in both Mann-Whitney-Wilcoxon and Kolmogorov-Smirnov tests). However, there was no apparent correlation between minimum turbidity current runout and water level, Homathko River discharge, and the cumulative river discharge (i.e. considering this as a proxy for sediment supply) between detected events (Fig. 5A-F). However, it is important to note that results are skewed towards shorter runout turbidity currents, with only three flows detected after MS4.

4.2. Predicting turbidity currents at Bute Inlet based on 2018 data

To examine the combined effect of Homathko River discharge and tides on turbidity current timing we fit the logistic regression model (Eq. (1)) to the turbidity currents recorded in 2018 (here N = 94 as two turbidity currents occurred within an hour; i.e. the resolution of Homathko River discharge and water level measurements). Fitting the 2018 dataset to the model quantifies the roles of the Homathko River discharge and water level such that:

$$\hat{p}(\mathrm{TC}) = \frac{e^{0.09Q+0.36L-0.52H-0.23hL-0.25lH-11.1}}{1+e^{0.09Q+0.36L-0.52H-0.23hL-0.25lH-11.1}}, \quad (2)$$

where parameters are the same as listed for Eq. (1). Our logistic analysis clearly reveals the controls played by both river discharge and tidal elevation. For example, turbidity current occurrence is at least 1.8 times more likely at low tide than any other position in the cycle for a given tidal range; and for every percentile increase in Homathko River discharge, the likelihood of a turbidity current increases by 9%.

By quantifying the roles of river discharge and tides on turbidity current generation (Eq. (2)) it is possible to predict the likelihood of turbidity current occurrence for any given river discharge and tidal conditions. Visual comparisons of between the output from Eq. (2) and the timing of ADCP observed turbidity currents demonstrates the good fit of the logistic model (Fig. 3D). For example, ADCP recorded turbidity currents generally coincide with higher predicted probabilities while periods of low predicted probabilities feature an absence of observed turbidity currents (Fig. 3D).

Statistical tests demonstrated the significance of our logistic model. For example, values of $p < 0.05$ and $\chi^2 > 11.1$ (the critical χ^2 value; Table 1) for both the likelihood ratio and Wald tests demonstrated the output of the logistic model had a stronger predictive power than random chance. Similarly, the Wald test showed the significance of each individual predictor variable with all having values of $p < 0.05$ and $\chi^2 > 3.84$ (the critical χ^2 value for a single variable; Table 1). The overall predictive power of the logistic model was assessed by comparing the frequency and timing between predicted turbidity current probabilities and actual monitored turbidity currents during 2018. The Hosmer-Lemeshow statistic ($p > 0.05$ and $\chi^2(8)$ below the critical value; see Supplementary Material) and McFadden pseudo-R^2

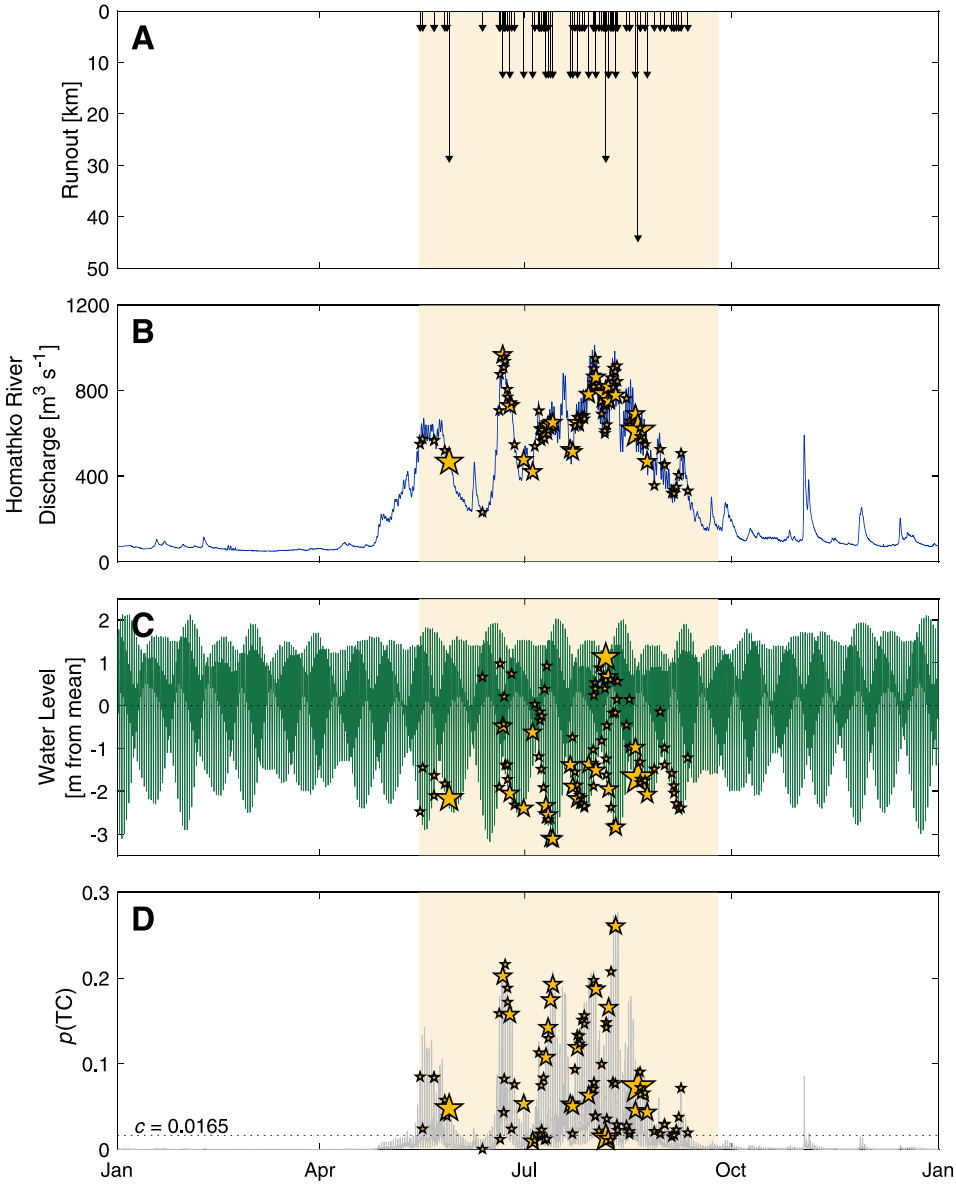

Fig. 4. Time series of recorded and calculated measurements during 2018 at Bute Inlet. (A) The timing of detected turbidity currents with minimum channel runout. (B) Homathko River discharge. (C) Deviation of water level from mean at Orford Bay. (D) Estimates for predicted probability of turbidity current occurrence from Eq. (2) using Homathko River discharge and water level recorded during 2018. Yellow stars in B-D show the value of each variable during measured turbidity currents, the size of star is relative to minimum flow runout. Zone highlighted in yellow denotes the period of instrument deployment, outside of which flow timing is unknown.

(R^2_{McF}) value above 0.2 (Table 1) indicate the overall predicted turbidity current frequencies were well calibrated to the actual monitored outcome, with the model showing good predictive power.

Model discrimination was assessed using a cut-point (c), above which the logistic model predicts the occurrence of a turbidity current, below the absence of a flow. Using the logistic model output with timing of ADCP monitored turbidity currents for 2018, the cut-point probability value (where sensitivity and specificity are equal; see Supplementary Material section A.3.4 and Fig. S1) was $c = 0.0165$. Using this cut-point the model was able to successfully predict 81 of the 95 ADCP recorded turbidity currents during 2018 as 'positive' events (i.e. the predicted probability for these turbidity currents was greater than c), with an overall model accuracy – for predicting events and non-events – of 86% (Fig. 3D; Table 2) for a year of Homathko River discharge and water level measurement inputs during 2018.

4.3. Model validation against 2016 monitoring data in Bute Inlet

The logistic model, which was based on the observed turbidity currents recorded in 2018, was then used to predict the probability of turbidity current occurrence in Bute Inlet from the 2016 monitoring campaign (i.e. data that were not used to train the model). Using the predetermined regression coefficients from Eq. (2), measurements of Homathko River discharge and water level for 2016 were used to calculate turbidity current probabilities, which could then be compared to the timing of ADCP monitored turbidity currents recorded during the 2016 instrument deployment campaign in Bute Inlet. Using the same predetermined cut-point ($c = 0.0165$), 17 of the 18 turbidity currents recorded during the 2016 instrument deployment were correctly predicted as positive. Overall the logistic model successfully predicted whether a turbidity current would occur, or not, with 90% accuracy through-

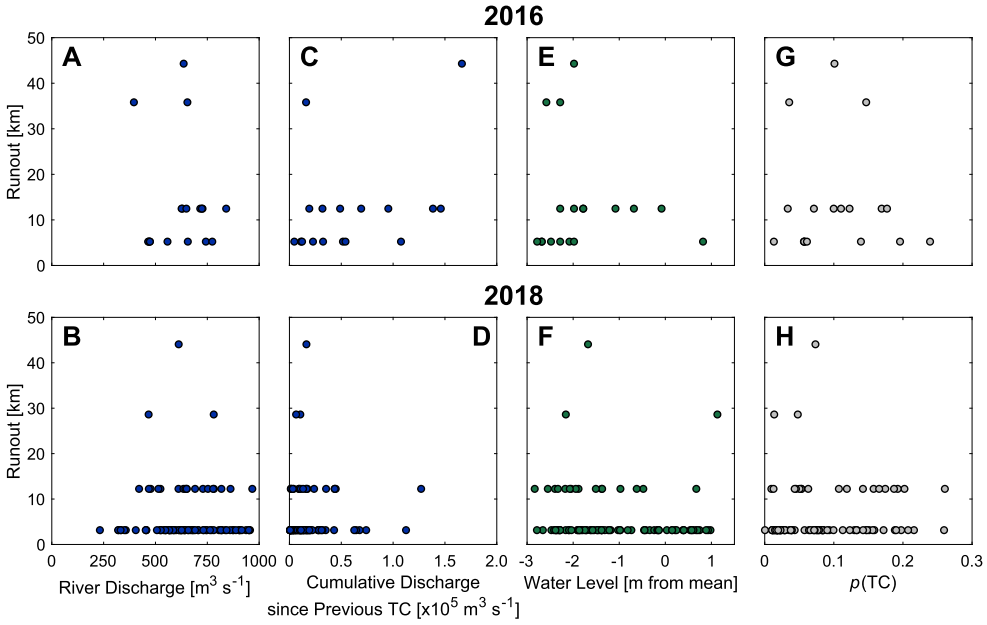

Fig. 5. Cross-plots to show the relationship between turbidity current runout and Homathko River discharge during (A) 2016 and (B) 2018; cumulative river discharge since the previous turbidity current during (C) 2016 and (D) 2018; water level during (E) 2016 and (F) 2018; and predicted probabilities from Eq. (2) during (G) 2016 and (H) 2018.

Table 1
Results of logistic regression analysis for turbidity current occurrence in Bute Inlet during 2018 with statistical analysis of individual predictors and the overall model. The calculated values for the constant (α) and each predictor (β) coefficient along with standard error (SE), Wald's χ^2, degrees of freedom (df), p-value and odds ratio (e^{β}). Results of the likelihood ratio, Wald and Hosmer and Lemeshow model evaluations and the McFadden pseudo-R^2 (R^2_{McF}) displayed. For more details of statistical tests see Supplementary Material.

Predictor	Coefficient	SE	Wald's χ^2	df	p	e^{β} [odds ratio]
Constant	-11.1050	0.8394	175.0056	1	< 0.0001	N/A
Homathko River Discharge	0.0880	0.0093	89.6649	1	< 0.0001	1.0920
L*tidal range	0.3582	0.0696	26.4898	1	< 0.0001	1.4308
hL*tidal range	-0.2279	0.1159	3.8687	1	0.0492	0.7792
lH*tidal range	-0.2538	0.1295	3.8430	1	0.0500	0.7759
H*tidal range	-0.5224	0.1720	9.2214	1	0.0024	0.5931

Test	χ^2	df	p
Likelihood ratio	360.1719	5	< 0.0001
Wald	155.0093	5	< 0.0001
Hosmer & Lemeshow	7.0204	8	0.5344

$R^2_{McF} = 0.2945$

Table 2
Predictive power of logistic model showing overall accuracy of turbidity current prediction of using cut point $c = 0.0165$ for training dataset (Bute Inlet 2018) and other test datasets. Sensitivity is the probability of predicting an observation as 'positive' given that a turbidity current was detected, and specificity is the probability of the model predicting a 'negative' given the actual outcome was no turbidity current detection. Overall accuracy calculated as the mean of sensitivity and specificity. TCs refer to turbidity currents.

Dataset	TCs [n]	Predicted TCs [$c > 0.0165$]	Sensitivity (%)	F (%)	Overall Accuracy (%)
Bute Inlet 2018	95	81	86.2	85.8	86.0
Bute Inlet 2016	18	17	94.4	85.4	89.9
Squamish Delta 2011	22	19	86.4	83.3	84.8
Fraser Delta 2008	3	3	100.0	84.2	92.1

out 2016 despite being trained on an independent dataset (Fig. 3D; Table 2).

4.4. Multivariate predictions outperform univariate predictions

The predictions from the logistic model were then compared to predictions from more simple univariate models made using either the Homathko River discharge or water level measurements in isolation to determine whether the multivariate approach is significantly more powerful. In isolation, river discharge and tidal water level are found to be poor predictors of turbidity current activity (Fig. 6). For example, when using Homathko River discharge alone to predict turbidity currents, a univariate model cannot predict the increased likelihood of a flow occurring at low tide, and hence

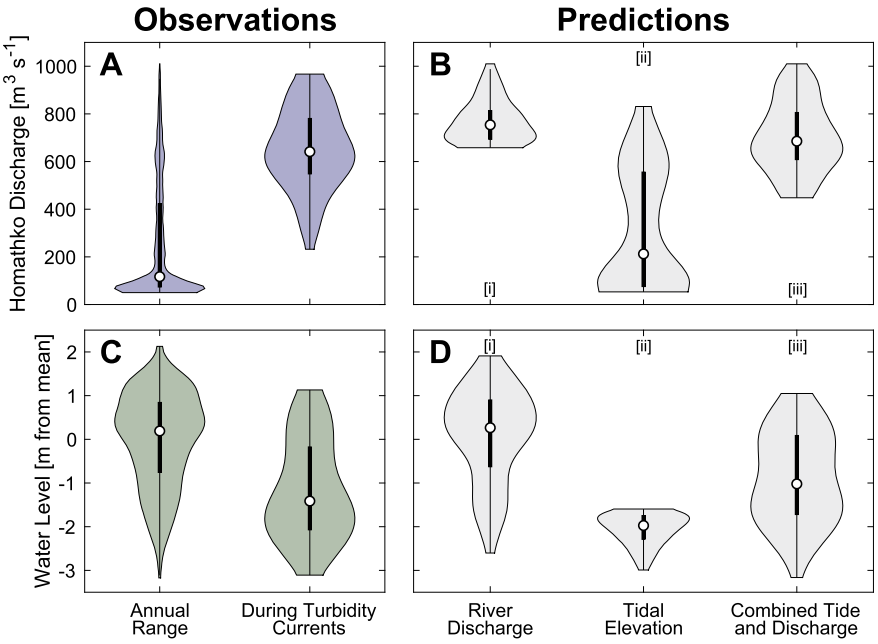

Fig. 6. Violin plots to compare the distribution of background forcing mechanisms with conditions during recorded turbidity currents, and different methods of prediction the occurrence of turbidity current activity at Bute Inlet during 2018. White filled circle shows median value for each data set and the thick central line represents the interquartile range. (A) The distribution of river discharge observations during 2018 with conditions during turbidity currents and (B) the distribution of conditions after predicting the timing of turbidity currents. (C) The distribution of water level observations during 2018 with conditions during turbidity currents and (D) the distribution of conditions after predicting the timing of turbidity currents. Turbidity current predictions were made by taking 95 random points in the top 10th percentile for Homathko River, the lowest 10th percentile in water level and top 10th percentile of the output from the predictive model. The plots in (B) and (D) show the distribution of Homathko River discharge (B) and water level (D) for each of the predictions, for example using (i) Homathko River discharge only, (ii) water level only, and (iii) the predictive model. For more details see Section 3.5.

misses a key mechanistic driver for flow triggering. In this case, the distribution of water level for turbidity currents predicted using Homathko River discharge alone showed no statistical difference ($p > 0.05$) to the annual distribution of water level measurements (Fig. 6; Table S2). Similarly, when water level alone was used to predict turbidity current timing, the model omitted the enhanced frequency of flows during short windows of elevated river discharge, and yielded no statistical difference to the annual range of river discharge ($p > 0.05$; Fig. 6; Table S2). However, the Homathko River discharge and water level during the 95 predicted turbidity currents using the logistic model showed no statistical difference ($p < 0.05$) to the actual Homathko River discharge and water level measurements during the ADCP recorded turbidity currents (Fig. 6; Table S2). Therefore, the logistic model, which incorporates both river discharge and tidal elevation, has a far stronger predictive power than univariate predictions that consider those variables in isolation.

5. Discussion

5.1. What explains the mismatches between reality and prediction?

Statistically, the logistic model shows strong predictive power for turbidity current occurrence, although there are discrepancies between predictions and observations. For example, a number of turbidity currents detected (one in 2016, and 13 in 2018) during the field deployments were not predicted by the multivariate model (i.e. predicted probability $> c$). We therefore now discuss why the model may not always correctly predict a turbidity current. We suggest that at least two potential mechanisms could lead to timing of a monitored turbidity current not being predicted as positive by the logistic model. First, a lag period may occur between elevated river discharge and delta-lip failure, such that an event may occur following a peak, when discharge levels are relatively low. Sediment can rapidly accumulate to prograde the delta-lip, or oversteepen the prodelta slope, during a short-lived period of elevated discharge, but not necessarily lead to immediate collapse. Instead these geometric effects or the generation of excess pore pressures in the subsurface may precondition the delta-lip to failure, with collapse occurring several hours to days later (Carter et al., 2012; Clare et al., 2016). River discharge can drop off during this lag phase, resulting in reduced predicted probabilities of turbidity current occurrence. Second, there may be a disconnect between river discharge and sediment input to the submarine channel head. Homathko River discharge is used as a proxy for sediment delivery to the delta-lip. When river discharge is elevated, the logistic model predicts increased likelihood of turbidity current activity (Eq. (2); Figs. 3; 4). However, bedload and/or suspended sediment flux do not increase linearly with discharge (Hickin, 1989). Additionally, the mouth bar located at the top of the delta can store large volumes of sediment which accumulates outside the freshet (Wright, 1977). Thus, the greater sediment availability (at the onset of the freshet) will increase the likelihood of a turbidity current (Bailey et al., 2021). This may also contribute to the longest runout (>40 km) turbidity currents recorded on the rising limb of the freshet hydrograph in both 2016 and 2018 (Figs. 3B; 4B). As such, the use of Homathko River discharge in the predictive model will result in an underestimation of turbidity current probabilities during the onset of the freshet. Similar predicted probability inaccuracies may also occur in late autumn. Here, storm related river flooding can discharge 10% of the annual suspended sediment load in a single day (Hickin, 1989). However, instruments were not deployed during this period so such a link cannot be tested with the available data.

The model also predicted turbidity currents during some periods in which no turbidity current was recorded. The logistic model predicts a likelihood value for a turbidity current with at least 2.8 km runout (i.e. runout to the most proximal mooring in 2018). However, high predictive probability, nor any triggering variable is always indicative of longer turbidity current runout

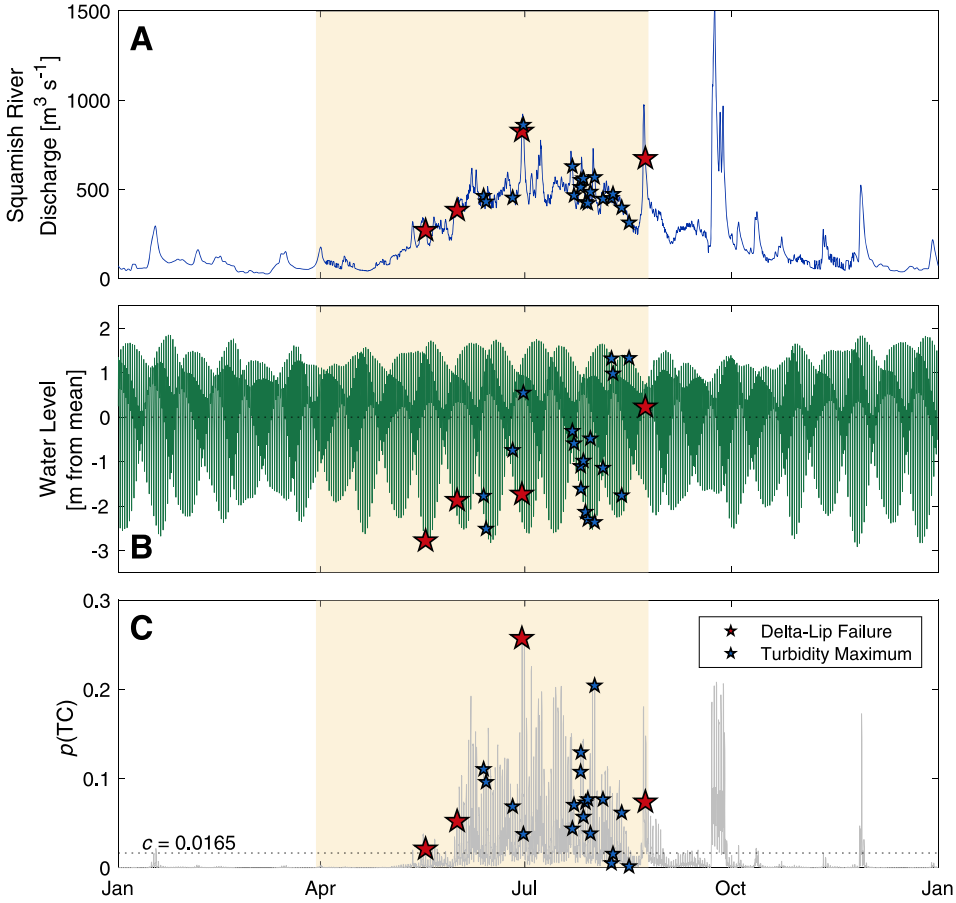

Fig. 7. Time series of recorded and calculated measurements at the Squamish Delta during 2011 (Hughes Clarke et al., 2012; Clare et al., 2016). (A) Squamish River discharge. (B) Deviations of water level from annual mean. (C) Estimates for predicted probability of turbidity current occurrence from Eq. (2) using measurements of Squamish River discharge and water level recorded during 2011. Stars in A-C denote the timing of ADCP measured turbidity currents, size and colour show mechanism of initiation, with instrument deployment period shown by highlighted zone.

(Fig. 5). Furthermore, observations of turbidity currents increase exponentially with proximity to the Homathko Delta (Pope et al., 2022). Similarly, up to seven individual turbidity currents were recorded during a single low tide period at the Squamish Delta-lip (Hughes Clarke, 2016). It is therefore plausible that turbidity currents did occur in the most proximal part of the channel (or on the prodelta itself) when predicted by the model, but did not run out sufficiently far for detection by our ADCP moorings. Additionally, despite high predicted probabilities, not every low tide during the deployment phase resulted in turbidity current generation (Figs. 3C, D; 4C, D). It has been proposed that low water sediment release from a turbidity maximum may also require the presence of sufficient erodible, unconsolidated sediment layer on the seafloor to generate a turbidity current. This layer may be removed following a turbidity current, inhibiting flow initiation at the following low tide (Hage et al., 2019). Our predictive model does not account for prior turbidity current occurrence and assesses flow likelihood independently based on triggering variables. As such, predicted probability in our model will remain elevated, even in the hours following a detected turbidity current.

5.2. Testing the predictive model at other deltas: Squamish and Fraser deltas

In the absence of major external triggers (e.g. earthquakes or large storms, Fig. S2), we are able to build a logistic model using variables linked to system preconditioning and flow initiation (river discharge and tidal state) to successfully predict >86% (Table 2) of the turbidity current activity at Bute Inlet. We therefore test our model using previous direct monitoring at the Squamish River and Fraser River Deltas. Previous univariate statistical analysis demonstrated that Squamish River discharge and water level had a significant control on turbidity current timing and rate; however, not all peaks in river discharge or low tide resulted in a turbidity current (Clare et al., 2016). We test the application of our logistic model (Eq. (2)) at Howe Sound by using Squamish River discharge and water level measurements recorded during 2011 to predict turbidity current likelihood and compare to the actual timing of the 22 ADCP recorded turbidity currents. Using the same cut-point determined for the 2018 Bute Inlet dataset ($c = 0.0165$), the model correctly predicted 19 of the 22 turbidity currents at Squamish as positive, with an overall model accuracy of 85% (assuming no turbidity currents occurred outside instrument deployment; Fig. 7; Table 2). Similarly, Fraser River discharge and water level measurements for 2008 were compared to the timing of three monitored turbidity currents during the same year. On this occasion, all three turbidity currents were successfully hindcast as 'positive' (Table 2). The logistic model shows good predictive power in, and can be applied to, systems where sediment supply is seasonal and turbidity currents are principally triggered at low tide. Furthermore, the ability to correctly hindcast turbidity current activity at the Fraser Delta demonstrates the model is not necessarily limited to smaller and bedload-dominant glacial-fed river systems.

5.3. Wider application to predict turbidity current activity in other river-fed systems

In this section, we discuss the application of our logistic model for turbidity current triggering by river discharge and tides to better quantify particulate fluxes at other systems worldwide. We suggest the model should have good predictive power for turbidity current activity in other glacial meltwater-fed fjords, such as those in Alaska, Greenland (Pope et al., 2019), Baffin Island (Normandeau et al., 2019), British Columbia (Gales et al., 2019), New Zealand (Strachan et al., 2016) and Patagonia (Dowdeswell and Vásquez, 2013; Vandekerkhove et al., 2020). Like Bute Inlet, these systems are all seasonally supplied by the same type of glacial sediment, have a similar geomorphology whereby deltas are sheltered from oceanographic processes (therefore sediment is not remobilised) and have a tidal influence. However, the validity may be compromised depending on the presence of proglacial lakes in the watershed. The number of watersheds where proglacial lakes are present is increasing (Shugar et al., 2020), and these features can trap sediment upstream, therefore hindering the supply of sediment to the marine nearshore environment and hindering turbidity current activity (Normandeau et al., 2019). Our predictive model assumes that river discharge is a proxy for sediment supply. This assumption cannot be robustly applied to watersheds where sediment is trapped upstream, here the use of the model would lead to an overprediction of turbidity current activity.

Several challenges exist for the wider application of our logistic model to non-glacial fed river deltas that border the open ocean. Deltas here may still be river discharge- or tidally controlled (Nienhuis et al., 2020). For example, recent monitoring of turbidity currents offshore the Congo River suggests that long runout (200-1,200 km) turbidity currents are associated with major river floods, with Spring tides being the ultimate trigger (Talling et al., 2022). Our model does not, however, account for oceanographic processes that affect continental margins that border open oceans (e.g. waves, internal currents or cascading dense-water; Puig et al., 2014). These processes will also likely influence turbidity current timing and triggering, and may have the further complication of supplying additional sediment through littoral cells (Bailey et al., 2021). To predict turbidity currents at deltas bordering the open ocean we must first understand the role of these additional forcing mechanisms. There is therefore a compelling need to monitor the timing of turbidity currents with greater precision, the oceanographic conditions adjacent to submarine canyons or channels, and to gather allied information on their runout distances, and a wider range of sites worldwide.

6. Conclusions

Two field campaigns in Bute Inlet during the freshet of 2016 and 2018 recorded 113 turbidity currents in a submarine channel. Here, we analyse the role of river discharge and tides on the generation of turbidity currents. In isolation, both elevation of Homathko River discharge and low tides showed statistical significance as turbidity current triggering mechanisms when compared to background conditions. The relative importance of each of these triggering variables was statistically evaluated using logistic regression on the timing of turbidity currents during 2018. Here, turbidity current occurrence was at least 1.8 times more likely at low tide than any other position in the cycle for a given tidal range; and for every percentile increase in Homathko River discharge, the likelihood of a turbidity current increased by 9%. Additionally, this logistic regression model was able to calculate turbidity current probability for any given input of Homathko River discharge and water level; successfully predicting 86% of turbidity current activity during 2018. We validate and demonstrate the good predictive power of our model by successfully predicting >84% of turbidity current activity for the 2016 monitoring dataset in Bute Inlet, and at other similar sites of direct monitoring (Squamish and Fraser Rivers). We suggest that our model can be further extended to predict turbidity current activity at other glacial-fed fjord-head deltas where river discharge can be used as a proxy for sediment delivery.

CRediT authorship contribution statement

Lewis P. Bailey: Conceptualization, Formal analysis, Methodology, Validation, Visualization, Writing – original draft. **Michael A. Clare:** Conceptualization, Funding acquisition, Methodology, Supervision, Validation, Writing – original draft. **Ed L. Pope:** Data curation, Methodology, Writing – review & editing. **Ivan D. Haigh:** Conceptualization, Methodology, Supervision, Writing – review & editing. **Matthieu J.B. Cartigny:** Writing – review & editing. **Peter J. Talling:** Funding acquisition, Writing – review & editing. **D. Gwyn Lintern:** Data curation, Funding acquisition, Writing – review & editing. **Sophie Hage:** Writing – review & editing. **Maarten Heijnen:** Writing – review & editing.

Declaration of competing interest

The authors declare that they have no known competing financial interests or personal relationships that could have appeared to influence the work reported in this paper.

Data availability

Data will be made available on request.

Acknowledgements

The crews and shipboard parties of the *RV John Strickland* and *CCGS Vector* are thanked for help in deploying and collecting the numerous moorings as part of this project. L.P.B. was supported by the Natural Environmental Research Council as part of the SPITFIRE Doctoral Training Program (Grant Number NE/L002531/1). M.A.C. was supported by the U.K. National Capability NERC Climate Linked Atlantic Sector Science program (NERC grant no. NE/R015953/1) and NERC grants (NE/P009190/1 and NE/P005780/1). E.L.P. was supported by a Leverhulme Trust Early Career Fellowship (ECF-2018-267). M.J.B.C. was supported by a Royal Society Dorothy Hodgkin Research Fellowship (DHF/R1/180166). S.H. has received funding from the European Union's Horizon 2020 research and innovation programme under the Marie Skłodowska-Curie grant agreement no. 899546. M.S.H. was funded under the Marie-Skłodowska-Curie grant agreement no. 721403–ITN Slate. We also acknowledge NERC funding (NE/M017540/1).

Appendix A. Supplementary material

Supplementary material related to this article can be found online at https://doi.org/10.1016/j.epsl.2022.117977.

References

Ayranci, K., Lintern, D.G., Hill, P.R., Dashtgard, S.E., 2012. Tide-supported gravity flows on the upper delta front, Fraser River delta, Canada. Mar. Geol. 326–328, 166–170. https://doi.org/10.1016/j.margeo.2012.09.007.

Bailey, L.P., Clare, M.A., Rosenberger, K.J., Cartigny, M.J.B., Talling, P.J., Paull, C.K., Gwiazda, R., Parsons, D.R., Simmons, S.M., Xu, J., Haigh, I.D., Maier, K.L., McGann, M., Lundsten, E., 2021. Preconditioning by sediment accumulation can produce powerful turbidity currents without major external triggers. Earth Planet. Sci. Lett. 562, 116845. https://doi.org/10.1016/j.epsl.2021.116845.

Bornhold, B.D., Ren, P., Prior, D.B., 1994. High-frequency turbidity currents in British Columbia fjords. Geo Mar. Lett. 14, 238–243. https://doi.org/10.1007/BF01274059.

Canals, M., Puig, P., de Madron, X.D., Heussner, S., Palanques, A., Fabres, J., 2006. Flushing submarine canyons. Nature 444, 354–357. https://doi.org/10.1038/nature05271.

Carter, L., Milliman, J.D., Talling, P.J., Gavey, R., Wynn, R.B., 2012. Near-synchronous and delayed initiation of long run-out submarine sediment flows from a record-breaking river flood, offshore Taiwan. Geophys. Res. Lett. 39. https://doi.org/10.1029/2012GL051172.

Christian, H.A., Woeller, D.J., Robertson, P.K., Courtney, R.C., 1997. Site investigations to evaluate flow liquefaction slides at Sand Heads, Fraser River delta. Can. Geotech. J. 34, 14.

Clare, M., Lintern, D.G., Rosenberger, K., Hughes Clarke, J.E., Paull, C., Gwiazda, R., Cartigny, M.J.B., Talling, P.J., Perara, D., Xu, J., Parsons, D., Jacinto, R.S., Apprioual, R., 2020. Lessons learned from the monitoring of turbidity currents and guidance for future platform designs. Geol. Soc. (Lond.) Spec. Publ. 500, 605–634. https://doi.org/10.1144/SP500-2019-173.

Clare, M.A., Hughes Clarke, J.E., Talling, P.J., Cartigny, M.J.B., Pratomo, D.G., 2016. Preconditioning and triggering of offshore slope failures and turbidity currents revealed by most detailed monitoring yet at a fjord-head delta. Earth Planet. Sci. Lett. 450, 208–220. https://doi.org/10.1016/j.epsl.2016.06.021.

Conway, K.W., Barrie, J.V., Picard, K., Bornhold, B.D., 2012. Submarine channel evolution: active channels in fjords, British Columbia, Canada. Geo Mar. Lett. 32, 301–312. https://doi.org/10.1007/s00367-012-0280-4.

Dai, M., Yin, Z., Meng, F., Liu, Q., Cai, W.-J., 2012. Spatial distribution of riverine DOC inputs to the ocean: an updated global synthesis. Carbon and nitrogen cycles, Curr. Opin. Environ. Sustain. 4, 170–178. https://doi.org/10.1016/j.cosust.2012.03.003.

Dowdeswell, J.A., Vásquez, M., 2013. Submarine landforms in the fjords of southern Chile: implications for glacimarine processes and sedimentation in a mild glacier-influenced environment. Quat. Sci. Rev. 64, 1–19. https://doi.org/10.1016/j.quascirev.2012.12.003.

Dyer, K.R., 1997. Estuaries: a Physical Introduction. Wiley, N. Y.

Eidam, E.F., Ogston, A.S., Nittrouer, C.A., 2019. Formation and removal of a coastal flood deposit. J. Geophys. Res., Oceans 124, 1045–1062. https://doi.org/10.1029/2018JC014360.

Gales, J.A., Talling, P.J., Cartigny, M.J.B., Hughes Clarke, J., Lintern, G., Stacey, C., Clare, M.A., 2019. What controls submarine channel development and the morphology of deltas entering deep-water fjords? Earth Surf. Process. Landf. 44, 535–551. https://doi.org/10.1002/esp.4515.

Galy, V., France-Lanord, C., Beyssac, O., Faure, P., Kudrass, H., Palhol, F., 2007. Efficient organic carbon burial in the Bengal fan sustained by the Himalayan erosional system. Nature 450, 407–410. https://doi.org/10.1038/nature06273.

Gavey, R., Carter, L., Liu, J.T., Talling, P.J., Hsu, R., Pope, E., Evans, G., 2017. Frequent sediment density flows during 2006 to 2015, triggered by competing seismic and weather events: observations from subsea cable breaks off southern Taiwan. Subaquatic paleoseismology: records of large Holocene earthquakes in marine and lacustrine sediments, Mar. Geol. 384, 147–158. https://doi.org/10.1016/j.margeo.2016.06.001.

Hage, S., Cartigny, M.J.B., Sumner, E.J., Clare, M.A., Hughes Clarke, J.E., Talling, P.J., Lintern, D.G., Simmons, S.M., Silva Jacinto, R., Vellinga, A.J., Allin, J.R., Azpiroz-Zabala, M., Gales, J.A., Hizzett, J.L., Hunt, J.E., Mozzato, A., Parsons, D.R., Pope, E.L., Stacey, C.D., Symons, W.O., Vardy, M.E., Watts, C., 2019. Direct monitoring reveals initiation of turbidity currents from extremely dilute river plumes. Geophys. Res. Lett. 46, 11310–11320. https://doi.org/10.1029/2019GL084526.

Hage, S., Galy, V.V., Cartigny, M.J.B., Acikalin, S., Clare, M.A., Gröcke, D.R., Hilton, R.G., Hunt, J.E., Lintern, D.G., McGhee, C.A., Parsons, D.R., Stacey, C.D., Sumner, E.J., Talling, P.J., 2020. Efficient preservation of young terrestrial organic carbon in sandy turbidity-current deposits. Geology 48, 882–887. https://doi.org/10.1130/G47320.1.

Hage, S., Galy, V.V., Cartigny, M.J.B., Heerema, C., Heijnen, M.S., Acikalin, S., Clare, M.A., Giesbrecht, I., Gröcke, D.R., Hendry, A., Hilton, R.G., Hubbard, S.M., Hunt, J.E., Lintern, D.G., McGhee, C., Parsons, D.R., Pope, E.L., Stacey, C.D., Sumner, E.J., Tank, S., Talling, P.J., 2022. Turbidity currents can dictate organic carbon fluxes across river-fed fjords: an example from Bute inlet (BC, Canada). J. Geophys. Res., Biogeosci. 127, e2022JG006824. https://doi.org/10.1029/2022JG006824.

Harris, P.T., Whiteway, T., 2011. Global distribution of large submarine canyons: geomorphic differences between active and passive continental margins. Mar. Geol. 285, 69–86. https://doi.org/10.1016/j.margeo.2011.05.008.

Heezen, B.C., Ewing, W.M., 1952. Turbidity currents and submarine slumps, and the 1929 Grand Banks [Newfoundland] earthquake. Am. J. Sci. 250, 849–873. https://doi.org/10.2475/ajs.250.12.849.

Heijnen, M.S., Clare, M.A., Cartigny, M.J.B., Talling, P.J., Hage, S., Lintern, D.G., Stacey, C., Parsons, D.R., Simmons, S.M., Chen, Y., Sumner, E.J., Dix, J.K., Hughes Clarke, J.E., 2020. Rapidly-migrating and internally-generated knickpoints can control submarine channel evolution. Nat. Commun. 11, 3129. https://doi.org/10.1038/s41467-020-16861-x.

Heijnen, M.S., Clare, M.A., Cartigny, M.J.B., Talling, P.J., Hage, S., Pope, E.L., Bailey, L., Sumner, E., Lintern, D.G., Stacey, C., Parsons, D.R., Simmons, S.M., Chen, Y., Hubbard, S.M., Eggenhuisen, J.T., Kane, I., Hughes Clarke, J.E., 2022. Fill, flush or shuffle: how is sediment carried through submarine channels to build lobes? Earth Planet. Sci. Lett. 584, 117481. https://doi.org/10.1016/j.epsl.2022.117481.

Hickin, E.J., 1989. Contemporary Squamish river sediment flux to Howe Sound, British Columbia. Can. J. Earth Sci. 26, 1953–1963. https://doi.org/10.1139/e89-165.

Hill, P.R., Lintern, D.G., 2021. Sedimentary processes at the mouth of a tidally-influenced delta: new insights from submarine observatory measurements, Fraser delta, Canada. Sedimentology 68, 2649–2670. https://doi.org/10.1111/sed.12868.

Hizzett, J.L., Hughes Clarke, J.E., Sumner, E.J., Cartigny, M.J.B., Talling, P.J., Clare, M.A., 2018. Which triggers produce the most erosive, frequent, and longest runout turbidity currents on deltas? Geophys. Res. Lett. 45, 855–863. https://doi.org/10.1002/2017GL075751.

Holland, R.S., 1976. Landforms of British Columbia: a Physiographic Outline. Br. Columbia Dept. Mines Pet. Res. Bull.

Howarth, J.D., Orpin, A.R., Kaneko, Y., Strachan, L.J., Nodder, S.D., Mountjoy, J.J., Barnes, P.M., Bostock, H.C., Holden, C., Jones, K., Cağatay, M.N., 2021. Calibrating the marine turbidite palaeoseismometer using the 2016 Kaikōura earthquake. Nat. Geosci. 14, 161–167. https://doi.org/10.1038/s41561-021-00692-6.

Hughes Clarke, J.E., Brucker, S., Muggah, J., Church, I., Cartwright, D., Kuus, P., Hamilton, T., Pratomo, D., Eisan, B., 2016. First wide-angle view of channelized turbidity currents links migrating cyclic steps to flow characteristics. Nat. Commun. 7, 11896. https://doi.org/10.1038/ncomms11896.

Hughes Clarke, J.E., Brucker, S., Muggah, J., Church, I., Cartwright, D., Kuus, P., Hamilton, T., Pratomo, D., Eisan, B., 2012. The Squamish ProDelta: Monitoring Active Landslides and Turbidity Currents 15.

Khripounoff, A., Vangriesheim, A., Crassous, P., Etoubleau, J., 2009. High frequency of sediment gravity flow events in the Var submarine canyon (Mediterranean Sea). Mar. Geol. 263, 1–6. https://doi.org/10.1016/j.margeo.2009.03.014.

Lee, H., Galy, V., Feng, X., Ponton, C., Galy, A., France-Lanord, C., Feakins, S.J., 2019. Sustained wood burial in the Bengal Fan over the last 19 My. Proc. Natl. Acad. Sci. 116, 22518–22525. https://doi.org/10.1073/pnas.1913714116.

Lemeshow, S., Hosmer Jr., D.W., 1982. A review of goodness of fit statistics for use in the development of logistic model regression. Am. J. Epidemiol. 115, 92–106. https://doi.org/10.1093/oxfordjournals.aje.a113284.

Lintern, D.G., Hill, P.R., Stacey, C., 2016. Powerful unconfined turbidity current captured by cabled observatory on the Fraser river delta slope, British Columbia, Canada. Sedimentology 63, 1041–1064. https://doi.org/10.1111/sed.12262.

Liu, J.T., Wang, Y.-H., Yang, R.J., Hsu, R.T., Kao, S.-J., Lin, H.-L., Kuo, F.H., 2012. Cyclone-induced hyperpycnal turbidity currents in a submarine canyon. J. Geophys. Res., Oceans 117. https://doi.org/10.1029/2011JC007630.

McFadden, D., 1974. The measurement of urban travel demand. J. Public Econ. 3, 303–328. https://doi.org/10.1016/0047-2727(74)90003-6.

Mulder, T., Syvitski, J.P.M., 1995. Turbidity currents generated at river mouths during exceptional discharges to the world oceans. J. Geol. 103, 285–299. https://doi.org/10.1086/629747.

Mulder, T., Syvitski, J.P.M., Migeon, S., Faugères, J.-C., Savoye, B., 2003. Marine hyperpycnal flows: initiation, behavior and related deposits. A review. Turbidites: Models and Problems, Mar. Pet. Geol. 20, 861–882. https://doi.org/10.1016/j.marpetgeo.2003.01.003.

Nienhuis, J.H., Ashton, A.D., Edmonds, D.A., Hoitink, A.J.F., Kettner, A.J., Rowland, J.C., Törnqvist, T.E., 2020. Global-scale human impact on delta morphology has led to net land area gain. Nature 577, 514–518. https://doi.org/10.1038/s41586-019-1905-9.

Normandeau, A., Dietrich, P., Hughes Clarke, J., Van Wychen, W., Lajeunesse, P., Burgess, D., Ghienne, J.-F., 2019. Retreat pattern of glaciers controls the occurrence of turbidity currents on high-latitude fjord deltas (Eastern Baffin Island). J. Geophys. Res., Earth Surf. 124, 1559–1571. https://doi.org/10.1029/2018JF004970.

Parsons, J.D., Bush, J.W.M., Syvitski, J.P.M., 2001. Hyperpycnal plume formation from riverine outflows with small sediment concentrations. Sedimentology 48, 465–478. https://doi.org/10.1046/j.1365-3091.2001.00384.x.

Peng, C.-Y.J., Lee, K.L., Ingersoll, G.M., 2002. An introduction to logistic regression analysis and reporting. J. Educ. Res. 96, 3–14. https://doi.org/10.1080/00220670209598786.

Pierdomenico, M., Casalbore, D., Chiocci, F.L., 2019. Massive benthic litter funnelled to deep sea by flash-flood generated hyperpycnal flows. Sci. Rep. 9, 5330. https://doi.org/10.1038/s41598-019-41816-8.

Pierdomenico, M., Ridente, D., Casalbore, D., Di Bella, L., Milli, S., Chiocci, F.L., 2022. Plastic burial by flash-flood deposits in a prodelta environment (Gulf of Patti, Southern Tyrrhenian Sea). Mar. Pollut. Bull. 181, 113819. https://doi.org/10.1016/j.marpolbul.2022.113819.

Piper, D.J.W., Cochonat, P., Morrison, M.L., 1999. The sequence of events around the epicentre of the 1929 Grand Banks earthquake: initiation of debris flows and turbidity current inferred from sidescan sonar. Sedimentology 46, 79–97. https://doi.org/10.1046/j.1365-3091.1999.00204.x.

Pohl, F., Eggenhuisen, J.T., Kane, I.A., Clare, M.A., 2020. Transport and burial of microplastics in deep-marine sediments by turbidity currents. Environ. Sci. Technol. 54, 4180–4189. https://doi.org/10.1021/acs.est.9b07527.

Pope, E.L., Cartigny, M.J.B., Clare, M.A., Talling, P.J., Lintern, D.G., Vellinga, A., Hage, S., Açikalin, S., Bailey, L., Chapplow, N., Chen, Y., Eggenhuisen, J.T., Hendry, A., Heerema, C.J., Heijnen, M.S., Hubbard, S.M., Hunt, J.E., McGhee, C., Parsons, D.R., Simmons, S.M., Stacey, C.D., Vendettuoli, D., 2022. First source-to-sink monitoring shows dense head controls sediment flux and runout in turbidity currents. Sci. Adv. 8, eabj3220. https://doi.org/10.1126/sciadv.abj3220.

Pope, E.L., Normandeau, A., Ó Cofaigh, C., Stokes, C.R., Talling, P.J., 2019. Controls on the formation of turbidity current channels associated with marine-terminating glaciers and ice sheets. Mar. Geol. 415, 105951. https://doi.org/10.1016/j.margeo.2019.05.010.

Prior, D.B., Wiseman, Wm.J., Gilbert, R., 1981. Submarine slope processes on a fan delta, Howe Sound, British Columbia. Geo Mar. Lett. 1, 85–90. https://doi.org/10.1007/BF02463323.

Puig, P., Palanques, A., Martín, J., 2014. Contemporary sediment-transport processes in submarine canyons. Annu. Rev. Mar. Sci. 6, 53–77. https://doi.org/10.1146/annurev-marine-010213-135037.

Shepard, F.P., 1972. Submarine canyons. Earth-Sci. Rev. 8, 1–12. https://doi.org/10.1016/0012-8252(72)90032-3.

Shugar, D.H., Burr, A., Haritashya, U.K., Kargel, J.S., Watson, C.S., Kennedy, M.C., Bevington, A.R., Betts, R.A., Harrison, S., Strattman, K., 2020. Rapid worldwide growth of glacial lakes since 1990. Nat. Clim. Change 10, 939–945. https://doi.org/10.1038/s41558-020-0855-4.

Strachan, L.J., Bostock, H.C., Barnes, P.M., Neil, H.L., Gosling, M., 2016. Non-cohesive silt turbidity current flow processes; insights from proximal sandy-silt and silty-sand turbidites, Fiordland, New Zealand. Sediment. Geol. 342, 118–132. https://doi.org/10.1016/j.sedgeo.2016.06.017.

Talling, P.J., 2014. On the triggers, resulting flow types and frequencies of subaqueous sediment density flows in different settings. In: 50th Anniversary Special Issue. Mar. Geol. 352, 155–182. https://doi.org/10.1016/j.margeo.2014.02.006.

Talling, P.J., Baker, M.L., Pope, E.L., Ruffell, S.C., Jacinto, R.S., Heijnen, M.S., Hage, S., Simmons, S.M., Hasenhündl, M., Heerema, C.J., McGhee, C., Apprioual, R., Ferrant, A., Cartigny, M.J.B., Parsons, D.R., Clare, M.A., Tshimanga, R.M., Trigg, M.A., Cula, C.A., Faria, R., Gaillot, A., Bola, G., Wallance, D., Griffiths, A., Nunny, R., Urlaub, M., Peirce, C., Burnett, R., Neasham, J., Hilton, R.J., 2022. Longest sediment flows yet measured show how major rivers connect efficiently to deep sea. Nat. Commun. 13, 4193. https://doi.org/10.1038/s41467-022-31689-3.

Vandekerkhove, E., Bertrand, S., Crescenzi Lanna, E., Reid, B., Pantoja, S., 2020. Modern sedimentary processes at the heads of Martínez channel and Steffen fjord, Chilean Patagonia. Mar. Geol. 419, 106076. https://doi.org/10.1016/j.margeo.2019.106076.

Wright, L.D., 1977. Sediment transport and deposition at river mouths: a synthesis. GSA Bull. 88, 857–868. https://doi.org/10.1130/0016-7606.

Zhong, G., Peng, X., 2021. Transport and accumulation of plastic litter in submarine canyons—the role of gravity flows. Geology 49, 581–586. https://doi.org/10.1130/G48536.1.